0026-895X/04/6503-558–570$20.00
MOLECULAR PHARMACOLOGY
Copyright © 2004 The American Society for Pharmacology and Experimental Therapeutics
Mol Pharmacol 65:558–570, 2004

Vol. 65, No. 3
3010/1134924
Printed in U.S.A.

Molecular Requirements of the Human Nucleoside Transporters hCNT1, hCNT2, and hENT1

C. Chang, P. W. Swaan, L. Y. Ngo, P. Y. Lum, S. D. Patil, and J. D. Unadkat

Biophysics Program, the Ohio State University, Columbus, Ohio (C.C.); Department of Pharmaceutical Sciences, University of Maryland at Baltimore, Baltimore, Maryland (P.W.S.); and Department of Pharmaceutics, University of Washington, Seattle, Washington (L.Y.N., P.Y.L., S.D.P., J.D.U.)

Received October 1, 2003; accepted December 8, 2003

This article is available online at http://molpharm.aspetjournals.org

ABSTRACT

Concentrative nucleoside transporters (CNTs) and equilibrative nucleoside transporters (ENTs) are important in physiological and pharmacological activity and disposition of nucleosides and nucleoside drugs. A better understanding of the structural requirements of inhibitors for these transporters will aid in designing therapeutic agents. To define the relative and unified structural requirements of nucleoside analogs for interaction with hCNT1, hCNT2, and hENT1, we applied an array of structure-activity techniques. Unique pharmacophore models for each respective nucleoside transporter were generated. These models reveal that hCNT2 affinity is dominated by hydrogen bonding features, whereas hCNT1 and hENT1 displayed mainly electrostatic and steric features. Hydrogen bond formation over 3′-OH is essential for all nucleoside transporters. Inhibition of nucleoside transporters by a series of uridine and adenosine analogs and a variety of drugs was analyzed by comparative molecular field analysis. Cross-validated r^2 (q^2) values were 0.65, 0.52, and 0.74 for hCNT1, hCNT2, and hENT1, respectively. The predictive quality of the models was further validated by successful prediction of the inhibition of a set of test compounds. Addition of a hydroxyl group around the 2-position of purine (or 3-position of pyrimidine) may increase inhibition to hCNT2 transporter; addition of hydroxyl group around the 2,7-position of purine (or the 3,5-position of pyrimidine) would increase the inhibition to hENT1 transporter. Utilization of these models should assist the design of high-affinity nucleoside transporter inhibitors and substrates for both anticancer and antiviral therapy.

Nucleoside transporters play an important role in physiology by regulating the extracellular concentration of adenosine and by salvaging nucleosides (Griffith and Jarvis, 1996). Nucleoside transporters can be divided into two broad classes (Cass et al., 1998), equilibrative and concentrative. Whereas hENT1 (*es*), a member of the equilibrative nucleoside transporters (ENTs), is expressed ubiquitously, Na^+-dependent concentrative transporters (CNTs) are found in more specialized tissues important for absorption (intestinal epithelia), distribution (blood-brain barrier), and elimination (hepatic and renal epithelia) of drugs. Among the nucleoside transporters, the purine specific concentrative nucleoside transporter (hCNT2), the pyrimidine specific concentrative nucleoside transporter (hCNT1), the nitrobenzylthioinosine-sensitive (hENT1) and -insensitive (hENT2) equilibrative transporters are expressed in the human intestinal epithelial cells (Chandrasena et al., 1997; Patil and Unadkat, 1997). Here they seem to be simultaneously expressed on different faces of the epithelial cells, mediating vectorial transport of nucleosides and nucleoside drugs (Lai et al., 2002).

Many antiviral (e.g., ribavirin) and anticancer nucleoside drugs (e.g., 5-fluorouridine) are substrates of nucleoside transporters (Jarvis et al., 1998). Their ability to transport nucleoside drugs is critical to the therapeutic effectiveness or toxicity of these drugs (Jarvis et al., 1998; Mackey et al., 1998). Therefore, understanding the basic molecular mechanism(s) of nucleoside transport should enable the design of more effective nucleoside drugs and those with better absorption profiles. Currently, the rational design of these drugs is hindered by the absence of high-resolution structural data on these transporters. For this reason, three-dimensional quantitative structure-activity relationships (3D-QSAR) can provide a helpful tool to direct the discovery of novel lead compounds with affinity for specific nucleoside transporters. This approach has been applied successfully to generate pharmacophore and 3D-QSAR models for the apical bile acid transporter (Swaan et al., 1997), peptide transporters (Swaan et al., 1998), P-glycoprotein (Ekins et al., 2002a,b), organic cat-

This research was funded by National Institutes of Health grants GM54447 (to J.D.U.) and DK56631 and DK061425 (to P.W.S.).

ABBREVIATIONS: ENT, equilibrative nucleoside transporter; CNT, concentrative nucleoside transporter; 3D, three-dimensional; QSAR, quantitative structure-activity relationship; CoMFA, comparative molecular field analysis; DISCO, distance comparisons; PLS, partial least squares; GOLPE, generating optimal linear PLS estimations; HB, hydrogen bond; MAPK, mitogen-activated protein kinase.

ion transporter 1 (Bednarczyk et al., 2003); for a recent review, see Zhang and et al. (2002). Previously, a limited QSAR model was developed to map the ENT transporter binding environment (Viswanadhan et al., 1990). At that time, specific information about the presence of different subtypes of nucleoside transporters was not available. Thus, this model represents the combined activities of equilibrative nucleoside transporters from various tissues and species (HL60 human leukemia cells, human red blood cells, L1210 mouse lymphocyte leukemia cells, guinea pig myocytes). Because hCNT1, hCNT2, and hENT1 are expressed in tissues important for drug disposition, in the current study we have generated distinctive pharmacophore models for each of these nucleoside transporters using the distance comparisons technique (Martin et al., 1993). We used inhibition profiles of hCNT2, hCNT1, and hENT1 transporters from our laboratory (Lum et al., 2000; Patil et al., 2000) to gain insight into the different binding mechanisms and requirements of these three nucleoside transporters. Subsequently, to generate 3D-QSARs, we performed comparative molecular field analysis (CoMFA) (Cramer et al., 1988), which provides subtle and unique structure-activity correlations for each individual nucleoside transporter. The quality of the models was assessed by their ability to successfully predict the inhibition of a set of test compounds. The current models enable us to predict transporter affinity and guide the design of novel lead compounds for drugs that may selectively target specific nucleoside transporter isoforms.

Materials and Methods

Biological Data. The biological (nucleoside uptake) data used here have been published previously (Lum et al., 2000; Patil et al., 2000). Briefly, the uptake of ^{3}H-labeled prototypic substrates of the hCNT2 (inosine, 0.5 μM), hCNT1 (thymidine, 1 μM), and hENT1 (uridine, 10 μM) transporters was measured in the presence and absence of various nucleosides and nucleoside analogs (Lum et al., 2000; Patil et al., 2000). The nucleoside analogs (Figs. 1–3) used were mostly analogs of uridine or adenosine and had a single substitution on either the sugar ring or the base or a single substitution on both rings. In addition, several nucleoside drugs (e.g., azidothymidine, cytarabine) were also tested. These uptake data, in the presence of inhibitors (0.1 mM for hCNTs and 2 mM for hENT1) used in the QSAR analysis were expressed as the percentage of the uptake obtained in the absence of these inhibitors. The hCNT1/2 studies were conducted with brush border membrane vesicles isolated from the human intestinal epithelia. Because both these transporters are expressed there, these studies could be conducted using the same vesicle preparations. We have previously shown that hCNT3 is not functionally expressed in the human intestinal epithelia (Ngo et al., 2001). The hENT1 studies were conducted with the *Xenopus laevis* oocytes expressing recombinant hENT1 (Lum et al., 2000). In the

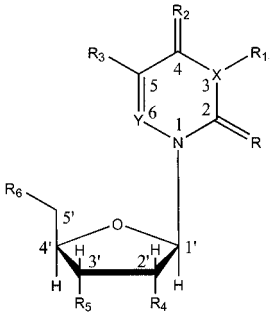

n	Name	X	Y	R	R_1	R_2	R_3	R_4	R_5	R_6
42	Uridine	N	C	O	H	O	H	OH	OH	OH
41	Thymidine	N	C	O	H	O	CH_3	H	OH	OH
13	3-Methyluridine	N	C	O	CH_3	O	H	OH	OH	OH
11	3-Deazauridine	C	C	O	H	O	H	OH	OH	OH
14	4-Thiouridine	N	C	O	H	S	H	OH	OH	OH
15	5-Bromouridine	N	C	O	H	O	Br	OH	OH	OH
52	5-Bromo-2′-deoxyuridine	N	C	O	H	O	Br	H	OH	OH
21	5-Fluorouridine	N	C	O	H	O	F	OH	OH	OH
23	5-Iodouridine	N	C	O	H	O	I	OH	OH	OH
49	5-Methyluridine	N	C	O	H	O	CH_3	OH	OH	OH
25	6-Azauridine	N	N	O	H	O	H	OH	OH	OH
8	2′-Deoxyuridine	N	C	O	H	O	H	H	OH	OH
12	3′-Deoxyuridine	N	C	O	H	O	H	OH	H	OH
4	2′,3′-Dideoxyuridine	N	C	O	H	O	H	H	H	OH
19	5-Fluoro-2′-deoxyuridine (Floxuridine)	N	C	O	H	O	F	H	OH	OH
20	5-Fluoro-5′-deoxyuridine (5′dFUrd)	N	C	O	H	O	F	OH	OH	H
22	5-Iodo-2′-deoxyuridine (Idoxuridine)	N	C	O	H	O	I	H	OH	OH
24	5-(Trifluoromethyl)-2′-deoxyuridine (Trifluridine)	N	C	O	H	O	CF_3	H	OH	OH
16	5-(2-Bromovinyl)-2′-deoxyuridine (Brivudin)	N	C	O	H	O	CH=CHBr	H	OH	OH
43	UMP	N	C	O	H	O	H	OH	OH	PO_4

Fig. 1. Chemical structures of uridine analogs and drugs used in QSAR analyses. The adenine base and deoxyribonucleoside groups are numbered for reference.

interest of brevity, the reader is referred to publications containing these data for further information (Lum et al., 2000; Patil et al., 2000).

Molecular Modeling and Structure Building. Computational studies were carried out on Octane and O_2 workstations (SGI, Mountain View, CA) with the IRIX 6.5 operating system running the SYBYL software suite version 6.7 (Tripos Associates, St. Louis, MO). Where crystal structures were not available, the starting geometry of nucleoside analogs was retrieved from the SYBYL Biopolymer database. When the analogs were not available from the database, the molecular structures of the inhibitors were built using standard bond distances and bond angles with the sketch module of SYBYL. The initial minimizations were performed using the Tripos force field with a distance-dependent dielectric coefficient and the Powell conjugate gradient algorithm with an energy change convergence criterion of 0.001 kcal/mol. Subsequently, the structural geometries were optimized with MOPAC (version 6.0) using the AM1 Hamiltonian and partial atomic charges (point charges) were assigned to all atoms.

DISCO. The distance comparisons (DISCO) module was used to generate pharmacophore maps for hCNT2, hCNT1, and hENT1 transporters. The method is based on the assumption that the pharmacological potency of a compound can be represented by its structural points of potential pharmacological interest, which are defined as "DISCO features" (e.g., hydrophobic centers or hydrogen bond donor atoms). A pharmacophore model is the final representation of the necessary 3D orientation of all chemical features (DISCO features) considered responsible for biological activity.

Not all nucleoside analogs were used in the analysis because DISCO assumes all input structures in a set are biologically active (i.e., can effectively inhibit nucleoside transport). Thus, only potent inhibitors, defined as compounds that can introduce a statistically significant ($p < 0.05$) change to the transporter affinity, were selected. To find the bioactive conformation instead of simply the energetically minimum conformation for each molecule, a maximum of 25 conformers within 70.0 kcal/mol energy cutoff were generated for each molecule using the MultiSearch function. DISCO features were assigned to all conformers. Based on the recommendation that the reference compound should be the molecule with few features and few conformers (Martin et al., 1993), we selected 2′-deoxyuridine, 5′-deoxythymidine, and 5′-deoxythymidine instead of a natural substrate as reference compounds for hCNT2, hCNT1, and hENT1 data sets, respectively. The feature distance tolerance was set at 1.0 Å. DISCO was initially run considering all the potential "feature" points. Additional runs with the specification of a minimum of two hydrophobic centers were also carried out. The resulting pharmacophore models were used to superimpose each set of the molecules.

FieldFit. A successful 3D-QSAR analysis requires the proper alignment of all compounds in the training and test sets. FieldFit was chosen to align target molecules to a template molecule so that their external (i.e., electrostatic) fields most closely resemble those of a template molecule. The template molecules for hCNT1, hCNT2, and hENT1 substrates are thymidine, inosine, and uridine, in that they represent model substrates for each data set; furthermore, these molecules were chosen as reference compounds in collecting experimental data (inhibition studies). The spring constant was set

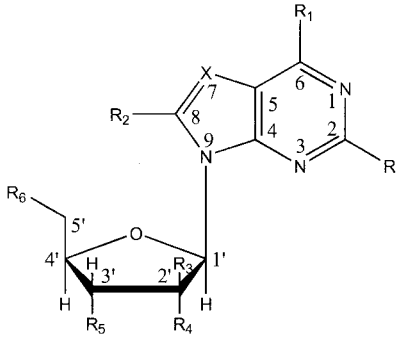

n	Compound	X	R	R_1	R_2	R_3	R_4	R_5	R_6
28	Adenosine	N	H	NH_2	H	H	OH	OH	OH
35	Inosine	N	H	OH	H	H	OH	OH	OH
34	Guanosine	N	NH_2	=O	H	H	OH	OH	OH
1	1-Methyladenosine [a]	N	H	=NH	H	H	OH	OH	OH
6	2-Chloroadenosine	N	Cl	NH_2	H	H	OH	OH	OH
47	2′-Deoxyguanosine	N	NH_2	=O	H	H	H	OH	OH
48	2′-Dideoxyinosine	N	H	OH	H	H	H	OH	OH
7	2′-Deoxyadenosine	N	H	NH_2	H	H	H	OH	OH
10	3′-Deoxyadenosine	N	H	NH_2	H	H	OH	H	OH
2	2′,3′-Dideoxyadenosine	N	H	NH_2	H	H	H	H	OH
33	2′,3′-Dideoxyinosine (ddI)	N	H	OH	H	H	H	H	OH
38	N^6-Methyladenosine	N	H	$NHCH_3$	H	H	OH	OH	OH
37	N^6,N^6-Dimethyladenosine	N	H	$N(CH_3)_2$	H	H	OH	OH	OH
26	7-Deazaadenosine	C	H	NH_2	H	H	OH	OH	OH
27	8-Bromoadenosine	N	H	NH_2	Br	H	OH	OH	OH
17	5′-Deoxyadenosine	N	H	NH_2	H	H	OH	OH	H
30	AF-adenine (Vidarabine)	N	H	NH_2	H	OH	H	OH	OH
5	2-Chloro-2′-deoxyadenosine (Cladribine)	N	Cl	NH_2	H	H	H	OH	OH
9	2-Fluoro-AF (Fludarabine)	N	F	NH_2	H	OH	H	OH	OH
51	Hypoxanthine	N	H	=O	H	H	OH	OH	OH
50	AF-hypoxanthine	N	H	=O	H	OH	H	OH	OH

[a] 1-Methyladenosine has a methyl moiety attached to N1; consequently, the N1-C6 double bond has shifted to the C6-R_1 position; AF=9β-D-Arabinofuranosyl

Fig. 2. Chemical structures of adenosine analogs and drugs used in QSAR analyses. The adenine/guanine base and deoxyribonucleoside groups are numbered for reference.

to 20 for all molecules. The resulting overlaps were analyzed by CoMFA and GOLPE.

CoMFA. CoMFA has proven to be an especially useful QSAR technique with considerable success in drug design and drug transport (Horwitz et al., 1994; Kroemer et al., 1998; Schaal et al., 2001; Swaan et al., 1997). It explains the gradual changes in observed biological properties by evaluating the electrostatic (Coulombic interactions) and steric (van der Waals interactions) fields at regularly spaced grid points surrounding a set of mutually aligned ligands for a specific target protein. A statistical algorithm, partial least squares (PLS), was used to correlate the field descriptors with biological activities. Both fields were calculated using an sp^3 hybridized carbon probe atom (+1 charge at 1.52-Å van der Waals radius) on a 2.0-Å spaced lattice, which extends beyond the dimensions of each nucleoside transport inhibitor by 4.0 Å in all directions. A cutoff of 30 kcal/mol ensures that no extreme energy terms will distort the final model. The indicator fields (Kroemer and Hecht, 1995) and hydrogen bond fields (Bohacek and McMartin, 1992) generated by the "advanced CoMFA" module are also included in the analysis. After the generation of field descriptors, a factor analysis is performed to help understand the clustering of inhibitors as well as locate potential outliers. CoMFA descriptors were used as independent variables, whereas the dependent variable (biological descriptor) used in these studies was the percentage inhibition of a reference compound for each individual transporter in the presence of a putative inhibitor. The experimental standard deviation was used as a weighting factor in PLS analyses, and calculation time was decreased by using sample-distance PLS. The predictive value of the models was evaluated first using leave-one-out cross-validation. The cross-validated coefficient, q^2, was calculated as follows:

$$q^2 = 1 - \frac{\sum_{Y}(Y_{predicted} - Y_{observed})^2}{\sum_{Y}(Y_{observed} - Y_{mean})^2} \quad (1)$$

where $Y_{predicted}$, $Y_{observed}$, and Y_{mean} are the predicted, observed, and mean values of the target property (percentage inhibition), respectively. $\Sigma(Y_{predicted} - Y_{observed})^2$ is the predictive error sum of squares. The standard error of the cross-validated predictions was known as *press*, and the root mean squares of the conventional (non–cross-validated) analysis was known as *s*. The model with the optimum number of PLS components, corresponding to the lowest predictive error sum of squares value was selected for deriving the final PLS regression models. In addition to q^2, the conventional correlation coefficient r^2 and its standard error were calculated. A plot of predicted versus experimental activity was used to identify potential outliers. The process was repeated until no further improvements in q^2 or no outliers could be identified. Results from alternative descriptor fields, such as *logP* and dipole moment, were compared and the model with the highest q^2 was accepted. A contour map of standard coefficients enclosing the top 20% lattice points where the QSAR strongly associates changes in CoMFA field values with changes in inhibition was created for each model.

The "predict properties" command in the QSAR module is used to predict the percentage inhibition of test compounds, which were selected from literature references (Graham et al., 2000; Lang et al., 2001; Vickers et al., 2002). The different environment in which the experimental data for the test set and training set compounds were obtained (i.e., different expression systems, substrate concentration, and inhibitor concentrations) does not allow for a direct comparison of predicted versus experimental values. Instead, the inhibitors are categorized into active (≤60% transport of the reference substrate in the presence of inhibitor) and inactive (>60%) inhibitors. Where only IC_{50} values are available (Vickers et al., 2002) (hENT1), a compound with an $IC_{50} \leq 2.0$ mM (1 μM substrate) is considered an active inhibitor, whereas a compound with an $IC_{50} > 2.0$ mM is considered an inactive inhibitor.

GOLPE. Generating Optimal Linear PLS Estimations (GOLPE; version 4.5, Multivariate Infometric Analysis, Perugia, Italy) is an alternative QSAR method that was used to validate independently the CoMFA results. It performs multivariate regression analysis on the interaction fields around the molecules generated by GRID19 (Goodford, 1985) (Molecular Discovery Ltd., Oxford, Great-Britain). The type of the field depends on the probe, which should be selected based on the type of the interested interaction. For our study, a phenolic hydroxyl (OH) probe was selected because it can offer both donor and acceptor of hydrogen bond as well as hydrophobic interaction. The interaction energies were calculated at 1.0-Å spaced grid points, which extended to be 4.0 Å beyond the dimensions of all the inhibitors. The generated interaction fields were selected and analyzed by GOLPE. A principal component analysis was performed to check the distribution of objects and variables. Four, five, and five maximal components were allowed in the principal component analysis of hCNT2, hCNT1, and hENT1 inhibitors, respectively. A conventional PLS was performed followed by a leave-one-out cross-validated PLS. A PLS plot (T-U plot) of the first component was generated to determine the outliers, which were excluded in the next run. The iteration was stopped when there were no obvious outliers in the PLS plot or no significant improvements in the result. Smart region design (Pastor et al., 1997) generated Voronoi polyhedra for

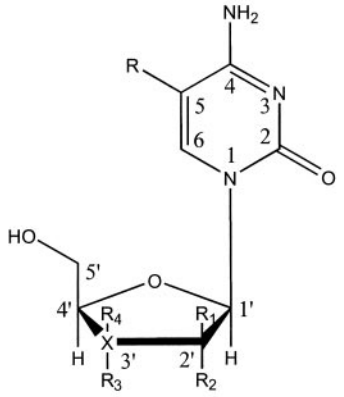

n	Compounds	X	R	R1	R2	R3	R4
32	Cytidine	C	H	H	OH	OH	H
46	2′-Deoxycytidine	C	H	H	H	OH	H
3	2′,3′-Dideoxycytidine	C	H	H	H	H	H
53	3′-Deoxycytidine	C	H	H	OH	H	H
31	9β-D-Arabinofuranosyl cytosine	C	H	OH	H	OH	H
45	Gemcitabine	C	H	F	F	OH	H
36	Lamivudine	S	H	H	H		
44	Zidovudine (AZT)	C	CH_3	H	H	N_3	H
40	Stavudine [a]	C	CH_3	H		H	

[a] Stavudine contains a double bond between 2′C and 3′C.

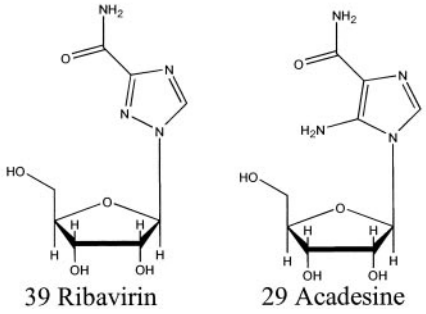

Fig. 3. Chemical structures of cytidine analogs and drugs used in QSAR analyses. The cytosine and deoxyribonucleoside groups are numbered for reference.

1000 seed variables around 1 grid unit region of each seed variable and then collapsed the polyhedra within 2 grid units of each seed variable. This maintains the three dimensional information and simplifies the following variable selection process. Based on smart region design, variables that best span the multidimensional weight space were selected by D-Optimal preselection. Fractional factorial design selection was carried out to further select only the most informative variables. The final conventional PLS was then performed followed by the cross-validated PLS. Coefficient contour maps enclosing the top 20% lattice points at which the QSAR strongly associates changes in GOLPE field values with changes in inhibition were generated for each model.

Results and Discussion

To gain an understanding of the binding mode of nucleoside analogs to their transporters, we used a computational approach to model in vitro affinity data. The program DISCO was used to generate pharmacophore models of the three-dimensional orientation of essential ligand characteristics that might ultimately relate to features within nucleoside transporters. These models were derived using multiple conformations of each individual ligand alongside the experimental inhibition data. The result is a computational model that can be used to predict the affinity of nucleoside analogs to each individual transporter and serve as a guide to the design of novel transporter inhibitors and ligands.

The structures of the nucleoside analogs used in this study are shown in Figs. 1 to 3, sorted by nucleobase moiety (adenine/guanine, thymine, and cytosine). Where available, trivial and registered drug names are listed. In previous literature, the 9β-D-arabinofuranosyl conformers of adenine, cytosine, and hypoxanthine have been named Ara-A, Ara-C, and Ara-H, respectively. The majority of DISCO feature points are located on the nucleoside pentose ring (Figs. 4, A–C). A detailed inspection shows that besides obvious similarities among the three individual transport pharmacophores, such as two hydrophobic centers and one hydrogen bond acceptor on the pentose ring, subtle differences set the individual transporters apart. For example, the presence of both a hydrogen bond acceptor and donor feature near 3′-C is important for hENT1 inhibitors (Fig. 4C); furthermore, hydrogen bond acceptors on 3′-OH and the 2-position of the

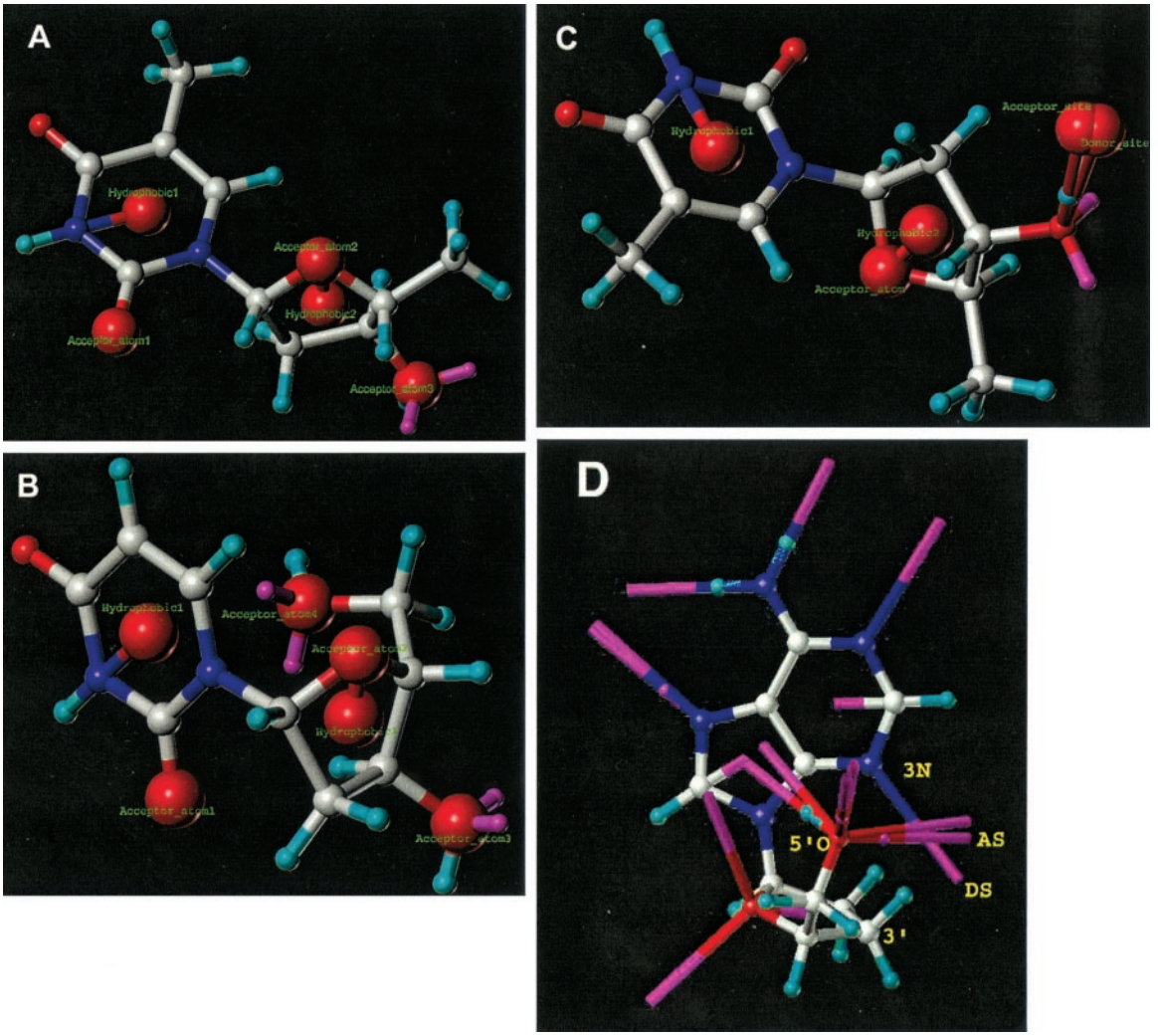

Fig. 4. Inhibition pharmacophore models for the three nucleoside transporters in relationship to the reference compound for each data set. A, hCNT1 is visualized in reference to its active inhibitor 5′-deoxythymidine; B, hCNT2 pharmacophore features are shown on 2′-deoxyuridine; and C, hENT1 pharmacophore moieties are presented on its substrate 5′-deoxythymidine. D, DISCO features of the hENT1 substrate and inhibitor 2′,3′-dideoxyadenosine, illustrating the hydrogen bond donor and acceptor site features of 3-N and 5′-OH, respectively, in the absence of a 3′-hydroxyl moiety. DISCO features are labeled and represented by red spheres.

pyrimidine ring are important for both hCNT1 and hCNT2 inhibitors (Fig. 4, A and B), whereas a hydrogen bond acceptor on 5′-OH is important only for hCNT2 inhibitors (Fig. 4B). In general, a pentose ring structure and hydrogen bond formation over 3′-C are necessary for a compound to effectively inhibit all three nucleoside transporters. This observation is consistent with the biological data, whereas the presence of 3′-OH is necessary for a nucleoside to be a high-affinity inhibitor or substrate of these transporters (Lum et al., 2000; Patil et al., 2000). Furthermore, a hydrogen bond acceptor at the 2-position of the pyrimidine ring is necessary for hCNT1 and hCNT2 inhibitors and an additional 5′-OH is required for hCNT2 inhibition. The interatomic distances between pharmacophore feature points are listed in Table 1, further illustrating similarities and distinct differences between the three transporter pharmacophore models. In general, interatomic distances between analogous pharmacophoric points are closely correlated (e.g., hydrophobic moiety 1–2, 3.69 ± 0.17 Å; acceptor atom 2-hydrophobic group 2, 1.20 ± 0.01 Å). Despite the distinct differences between the three transporters, there are molecules that adhere to all three requirements and will therefore exert affinity for all transporter isoforms, such as uridine and adenosine.

A pharmacophore is a useful approach to analyze the chemical groups and their three-dimensional orientation required for biological activity; however, it takes into consideration only *active* molecules, even though *inactive* molecules could further delineate the chemical boundaries of designing transport inhibitors. Furthermore, pharmacophore models generally do not take into consideration potential electrostatic and steric interactions. To address these limitations, we extended our analyses using the 3D-QSAR algorithms CoMFA and GOLPE. After excluding eventual outliers in an iterative process, predictive QSAR models were derived for each of the individual nucleoside transporters (Table 2). As a further illustration, C and D in Figs. 5 to 7 display the residual plots of divergence between predicted and actual activity values for the hCNT1, hCNT2, and hENT1 models, respectively. The CoMFA models feature robust q^2 values (0.65 for hCNT1, 0.516 for hCNT2, and 0.739 for hENT1), indicative of an internally consistent model.

TABLE 1

Intramolecular atomic distances between pharmacophoric feature points

All distances in Ångstroms. See Fig. 4, A–C, for details on relative positioning of pharmacophore features on representative ligands.

hCNT1	Hydr2	AA1	AA2	AA3	
Hydr1	3.79[a]	2.59	3.60	6.02	
Hydr2		3.94	1.20	2.56	
AA1			4.00	5.97	
AA2				3.58	
hCNT2	Hydr2	AA1	AA2	AA3	AA4
Hydr1	3.49	2.95	3.52	5.54	2.75
Hydr2		3.17	1.19	2.54	2.88
AA1			3.97	4.32	3.65
AA2				3.50	2.99
AA3					4.14
hENT1	Hydr2	AA	AS	DS	
Hydr1	3.79	3.60	7.00	7.21	
Hydr2		1.20	4.75	4.86	
AA			5.90	6.01	
DS				0.26	

AA, acceptor atom; Hydr, hydrophobic atom; AS, acceptor site; DS, donor site.

The biological implications of the QSAR analyses are explained through CoMFA coefficient contour maps (A, Figs. 5–7), which illustrate the correlation of steric and electrostatic fields with biological activity. An exception is the map of hCNT2, which visualizes the hydrogen bond aspect, in that this parameter correlates better with biological data (Fig. 6A). A model substrate for each transporter is displayed within the contour map to facilitate interpreting the relative positioning of the CoMFA fields. The polyhedra in each map surround all lattice points at which the QSAR strongly associates changes in interaction field values with changes in biological activity (i.e., percentage inhibition). The contours of the steric map (or hydrogen bond acceptor field map) are shown in yellow and green, and those of the electrostatic map (or hydrogen bond donor field map) are shown in red and blue. Greater inhibition is correlated with less bulk (weaker H-bond acceptor) near green, more bulk (stronger H-bond acceptor) near yellow, more negative charge (stronger H-bond donor) near blue, and more positive charge (weaker H-bond donor) near red.

The CoMFA plot for hCNT1 (Fig. 5A), reveals the presence of blue contours spanning both 3′- and 5′-OH, indicating the importance of electronegative charge around these two positions and their critical role in hCNT1 transporter inhibition. An additional advantage of CoMFA over pharmacophore mapping is evident here: the 5′OH is not identified in the hCNT1 pharmacophore model because 5′-deoxyadenosine is an active inhibitor; however, the low affinity for the transporter (26.5% inhibition of reference substrate) is weighed appropriately in CoMFA and correlated with the absence of a 5′-OH. The red contour over the 3,6-position of the pyrimidine ring indicates more positive groups on these positions will contribute to stronger inhibition of hCNT1, whereas a blue contour under the 6-position of the pyrimidine ring indicates that negative groups correlate better with hCNT1 transporter inhibition. Therefore, substituting hydrogen with a hydroxyl group at the 6-position of the pyrimidine base would satisfy both requirements. The green contour over the nucleoside base ring (Fig. 5A), which would suggest that less bulk in this general area could result in a molecule with higher affinity to hCNT1, is predominantly produced by 8-bromoadenosine (data not shown). The base ring of 8-bromoadenosine is aligned out of the plane formed by all other compounds (not shown) and the algorithm, which can be sensitive to molecular overlap, inaccurately correlates this bulk with its low inhibitory capacity. We can therefore conclude that this polyhedron is an artifact of the molecular overlapping algorithm.

The hCNT2 CoMFA model (Fig. 6A) differs from the hCNT1 model in that biological activity is correlated exclusively to hydrogen bond (HB) fields compared with a combination of steric, electrostatic (CoMFA), and hydrogen bond (GOLPE) fields for hCNT1. Inspection of the hCNT2 field contour map reveals a predominance of hydrogen bond donor polyhedra (blue contours), suggesting that active inhibitors of hCNT2 feature multiple hydrogen bond donor groups. Conversely, this indicates that the binding site of the hCNT2 transporter protein may be rich in amino acids with strong hydrogen bond acceptor features, such as Thr, Ser, Gln, or Asn. Loewen (1999) showed that a highly conserved putative binding domain confers pyrimidine selectivity to hCNT1 containing Ser319/Gln320 and Ser353/Leu354; when these

amino acids were mutated to their corresponding residues in hCNT2 (Gly313/Met314 and Thr347/Val348), the resulting transporter became purine-selective. Additional point mutations had variable effects on the purine and pyrimidine selectivity of both transporters. For example, the hCNT1/S319G/Q320M/S353T/L354V mutant conferred full hCNT2 transport characteristics, even though mutation of Ser319 of hCNT1 to Gly by itself enabled transport of purine nucleosides. Although the S353G mutation may imply that, relative to hCNT2, the hCNT1 binding domain comprises more hydrogen bond-forming amino acid residues, most mutations exchanged amino acids of similar properties. Overall, these

TABLE 2
Statistical parameters for 3D-QSAR analyses

Type	q^2	*press*	r^2	*s*	#[c]	% Steric	% Electrostatic
CoMFA							
hCNT1	0.65	25.91	0.98	6.04	5	0.46	0.54
hCNT2	0.52	24.33	0.83	14.5	2	0.51[a]	0.49[b]
hENT1	0.74	21.50	1.00	2.10	8	0.47	0.53
GOLPE							
hCNT1	0.69	20.20	0.89	12.00	3		
hCNT2	0.69	18.42	0.96	6.94	5		
hENT1	0.70	20.11	0.92	10.23	4		

[a] %HB acceptor for hCNT2.
[b] %HB donor for hCNT2.
[c] Number of components used for non–cross-validated analyses

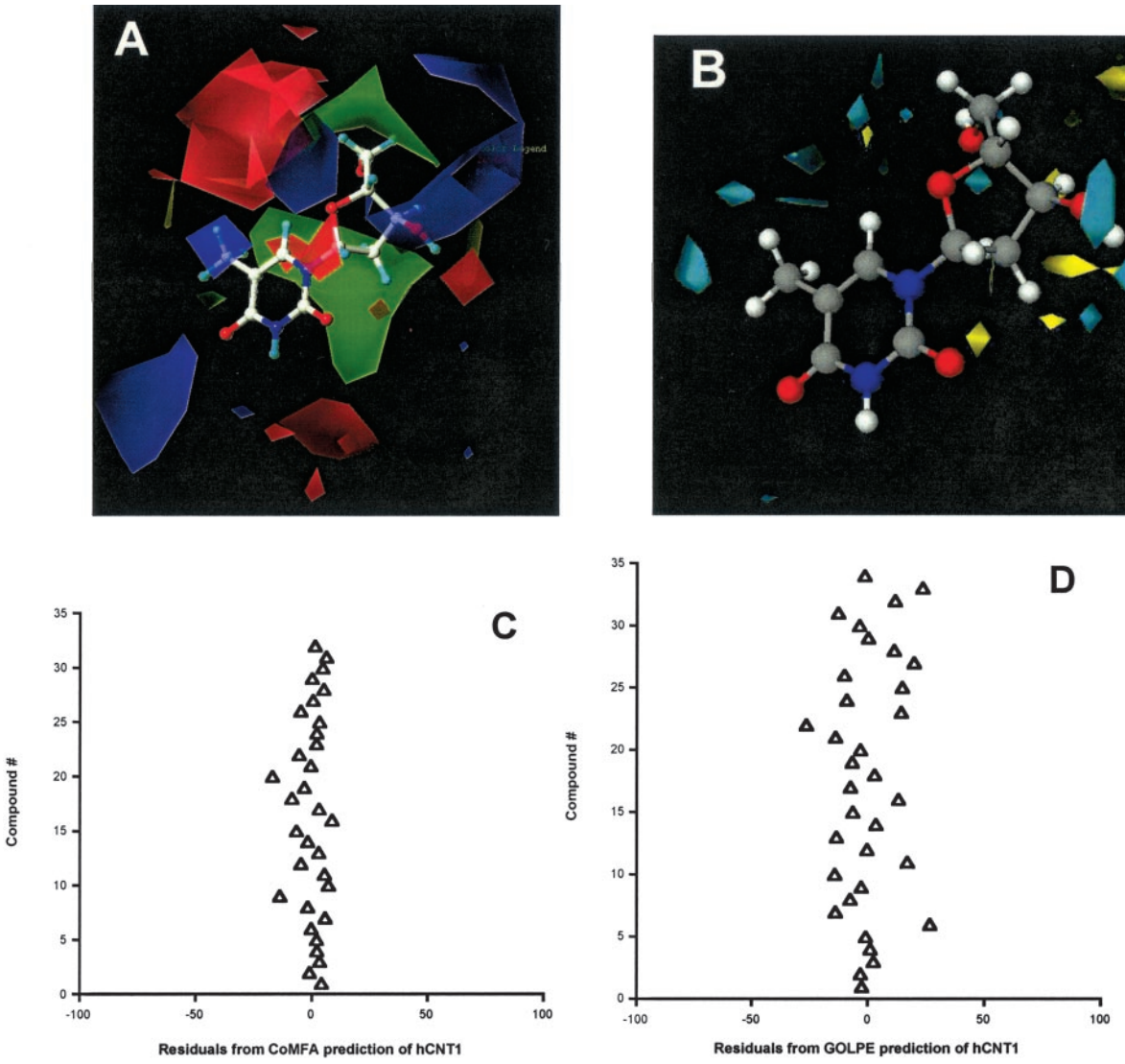

Fig. 5. 3D-QSAR model of nucleoside transporter hCNT1. A, CoMFA coefficient contour map surrounding model substrate thymidine illustrating the correlation of CoMFA fields with biological activity. Steric contour maps indicate greater inhibition is correlated with less steric bulk near green contours and more steric bulk near yellow. Electrostatic contours suggest that more negative electrostatic charge near blue and more positive charge near red will increase biological activity. B, GOLPE coefficient contour map illustrating the correlation of hydrogen bond acceptor (cyan) and donor (yellow) fields with percent inhibition. C, CoMFA residual plot indicating correlation and internal consistency of the model. D, GOLPE residual plot.

studies do not agree or disagree with our prediction that hCNT2 inhibition is governed predominantly by amino acids capable hydrogen bond formation. As suggested by the authors (Loewen et al., 1999), some mutants may exert their effects through altered helix packing, thereby indirectly affecting substrate specificity of the transport translocation domain. Clearly, these ligand-protein interaction effects fall outside the scope of extrapolation possible with our current analysis.

The blue contour (Fig. 6A, α field) under the 3′ and 5′ positions of the sugar ring of hCNT2 emphasizes the importance of the 3′-H and 5′-OH as HB donors. The green contour, γ, under the 5′ and 1′ positions emphasizes the role of 1′-O and 5′-OH as HB acceptor features. The blue contour, designated β (Fig. 6A), over 3′-OH emphasizes the importance of 3′OH in its role as a HB donor for affinity toward hCNT2. Overall, these data emphasize the importance of the 3′ hydrogen and hydroxyl as well as the 5′ hydroxyl groups for effective hCNT2 transporter inhibition, which correlates well with the pharmacophore model (Fig. 4B). From this model, we can expect a higher inhibition if more potent HB donating groups were placed around the purine base at the 2-position or possibly the 1-, 6-, or 7-position (groups R, R_1, and X in Fig. 2). For example, a hydroxyl group could satisfy both HB acceptor (green) and HB donor (blue) fields around the 2-position of the purine base. These guidelines can aid in the future design of compounds that selectively inhibit hCNT2.

Analogous to hCNT1, the biological activity of hENT1 inhibitors correlates well with steric and electrostatic fields (Fig. 7A). The large blue contour over the 3′ position of the pentose moiety indicates the importance of a hydroxyl group for affinity to the hENT1 transporter. Whereas hCNT1 and hCNT2 displayed blue contours over the 5′ and 2′ positions, these are not present in hENT1, indicating the relative in-

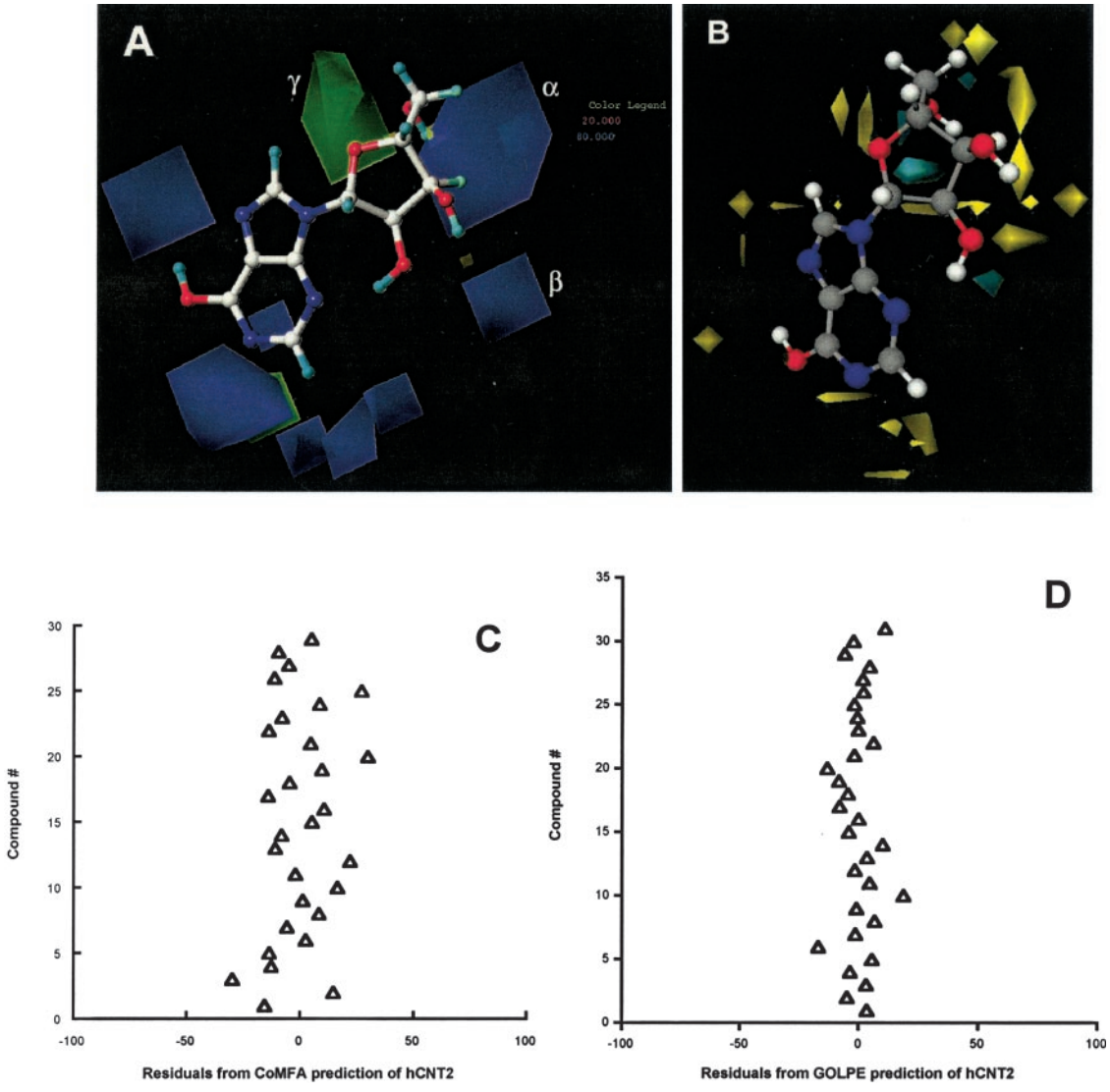

Fig. 6. 3D-QSAR model of the nucleoside transporter hCNT2. A, CoMFA coefficient contour map surrounding model substrate inosine illustrating the correlation of CoMFA fields with biological activity. The polyhedra in each map surround all lattice points where the QSAR strongly associates changes in interaction field values with changes in biological activity (i.e., percentage inhibition). The contours of the hydrogen bond acceptor field map are shown in yellow and green and those of the hydrogen bond donor field map are shown in red and blue. Greater inhibition is correlated with weaker H-bond acceptor near green, stronger H-bond acceptor near yellow, stronger H-bond donor near blue, and weaker H-bond donor near red. B, GOLPE coefficient contour map illustrating the correlation of hydrogen bond acceptor (cyan) and donor (yellow) fields with percentage inhibition. C, CoMFA residual plot indicating correlation and internal consistency of the model. D, GOLPE residual plot.

sensitivity of hENT1 transporter toward 2′- and 5′-OH. The red contour over the 2,7-position of purine (or the 3,5-position of pyrimidine) indicates that more electropositive groups at these positions will contribute to higher affinity (i.e., inhibition) of hENT1. At the same time, the blue contour over the purine (pyrimidine) ring suggests the existence of more negative groups near the 1,2,6,7-position of purine or the 3,4,5-position of pyrimidine. A combination of these two criteria (i.e., addition of a hydroxyl group at 2,7-position of purine or 3,5-position of pyrimidine) would aid in developing more potent inhibitors of hENT1 transport. Addition of a hydroxyl group at the 7-position of purine is chemically unfeasible, but because of the inexact nature of QSAR models, addition of a hydroxyl group at the 8-position of the purine substructure might generate the same effect. Although such compounds are not commercially available, future studies may use these findings in the design of novel compounds for hENT1. The green contours above and below the 1,7-position of purine (or 4,5-position of pyrimidine) suggest less bulky groups on these positions might lead to higher inhibition of hENT1. As noted before, however, these data could be the result of overlapping artifacts and should be interpreted with caution.

The divergence of predicted from experimental data are presented in residual plots for the respective CoMFA analyses (Figs. 5C, 6C, and 7C) and allow inspection of the internal consistency of the models. From these plots, it is apparent that the hCNT2 model has significantly more scatter than those of hCNT1 and hENT1, which is accurately reflected by their q^2 and r^2 values.

The GOLPE analyses assisted in further validating the biological implications of CoMFA models. The resulting GOLPE models are statistically robust, as indicated by their q^2 values (0.69 for hCNT1, 0.69 for hCNT2, and 0.70 for hENT1). GOLPE differs from CoMFA in the utilization of its probe atom, a phenolic hydroxyl group capable of donating and accepting one hydrogen bond, allowing for an alternative interpretation of coefficient contours. The GOLPE analyses can correlate biological activity with hydrogen bonding patterns. Because the OH probe is partially negative, its interaction with hydrogen bond donors will be favorable (yellow

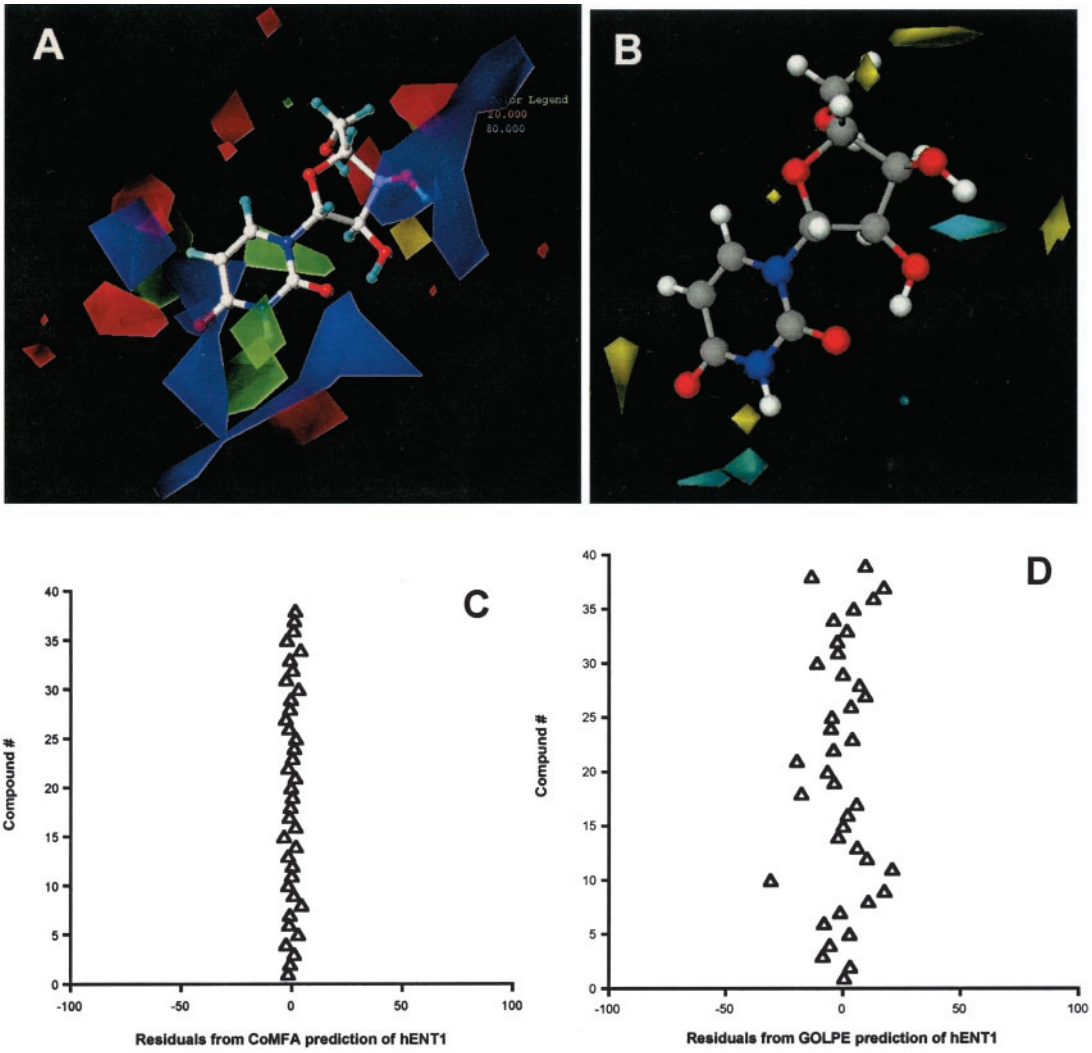

Fig. 7. QSAR model of hENT1. A, CoMFA coefficient contour map around the model compound uridine illustrating the correlation of CoMFA fields with percentage inhibition. Steric contour maps indicate that greater inhibition is correlated with less steric bulk near green contours; more steric bulk near yellow. Electrostatic contours suggest that more negative electrostatic charge near blue, and more positive charge near red will increase biological activity. B, GOLPE coefficient contour map illustrating the correlation of hydrogen bond acceptor (cyan) and donor (yellow) fields with percent inhibition. C, CoMFA residual plot indicating correlation and internal consistency of the model. D, GOLPE residual plot.

contours) and its interaction with hydrogen bond acceptor will be unfavorable (cyan contours).

The hCNT1 contour map (Fig. 5B), reveals a yellow contour over 3′-(O)H and a cyan contour over 3′-O(H), emphasizing significance of HB donation at 3′-(O)H and HB acceptance at 3′-O(H), and further implying an important role for the dual HB donor/acceptor character of the 3′-OH in affinity for the hCNT1 transporter. This agrees with both the pharmacophore model and CoMFA result. On the other hand, GOLPE does not display a correlation with the 5′-OH group that CoMFA revealed. The small yellow contour over the 6-position of pyrimidine emphasizes the importance of hydrogen bond donor, whereas several cyan contours over the same position emphasize the importance of hydrogen bond acceptor. A substitution of -H by -OH at the 6-position of pyrimidine would provide both hydrogen bond donor and acceptor. This GOLPE prediction is in good agreement with suggestions from the above CoMFA analyses, further emphasizing the complementary and sometimes supplementary character of two independent 3D-QSAR techniques.

The hCNT2 GOLPE data (Fig. 6B) show distinct yellow contours over 5′-(O)H, 3′-(O)H, and 3′-H, indicating that both 3′-(O)H and 5′-(O)H are essential in maintaining inhibition. The cyan contours over 3′-O(H) and 5′-O emphasize the importance of 3′,5′-O for hCNT2 transporter inhibition. GOLPE confirms the importance of both 3′- and 5′-OH, which were previously identified by the pharmacophore and CoMFA models. The GOLPE contour plot, however, provides more detailed and punctate fields that can be associated with specific moieties on the substrate molecule. The yellow contours over the nucleobase ring follow a similar pattern compared with the HB CoMFA model. In particular, the yellow contour flanking the 2 position of purine (favoring a hydrogen bond donor on 2 position) confirms the previous CoMFA prediction that 2-OH substitution of 2-H of purine could increase affinity toward hCNT2.

The yellow contours over 3′-(O)H, as well as the cyan contour over 3′-O(H), emphasize the importance of the 3′ position in inhibiting the hENT1 transporter (Fig. 7B). Hydrogen-bonding fields are not detected over 2′- and 5′-OH, which is in good agreement with the pharmacophore and CoMFA models. At the nucleobase side, two yellow contours over the 3,5-position of pyrimidine (or, analogously, the 2,7-position of purine) suggest that HB forming in these two positions will increase inhibition, again confirming the above CoMFA predictions. The cyan contour near the 3-position of pyrimidine provides additional confirmation of the putative positive effect of 3-hydroxyl substitution on hENT1 inhibition.

The models were subsequently used to predict the inhibition capacity of a set of test compounds (Table 4). Predictions agree with experimentally determined inhibition profiles except for 9-β-D-arabinofuranosyl(AF)-hypoxanthine. Contrary to literature data (Lang et al., 2001), our model predicts this particular compound as an inactive hCNT2 inhibitor, but it *correctly* predicts hypoxanthine to be inactive. It is important to point out, however, that the AF analogs in our training set [i.e., compounds 9 (Fludarabine) and 30 (vidarabine)], which bear a hydroxyl group at the 2′ position of the pentose moiety in the α conformation, are not active hCNT2 inhibitors (Molina-Arcas et al., 2003). Conversely, analogs comprising a β-2′-OH moiety (e.g., adenine) are active inhibitors of hCNT2. Intrinsically, the model can only extrapolate from the data within the training set, which signifies that the model will correlate a compound containing a α-2′-OH as inactive toward hCNT2. The observation by Lang et al. (2001) that AF-hypoxanthine is an active inhibitor for hCNT2 could be the result of different experimental conditions. For example, both AF-adenine (31%) and adenosine (2%) were reported to be active hCNT2 inhibitors, whereas our data (Patil et al., 2000) show AF-adenine to be inactive toward hCNT2.

Overall, steric and electrostatic interactions play an important role in hCNT1 and hENT1 inhibition, whereas hydrogen bonding is dominant in hCNT2 inhibition. Despite their differences, all three QSAR models identified the essential role of the 3′ hydroxyl group as essential for inhibiting nucleoside transporters. In addition, the 5′-OH was identified as important for hCNT1 and hCNT2 transporter inhibition. The hENT1 transporter is more tolerant to hydroxyl group substitution on the pentose ring than the other two transporters. A recent study by Zhang et al. (2003) on uridine-binding motifs of hCNT1 and hCNT3 concluded that the following groups determined substrate affinity for hCNT1 in decreasing sensitivity: C(3′) > C(5′) = N(3) > C(2′). This study is in good agreement with the DISCO-generated pharmacophore points for hCNT1 (i.e., both 3′- and 5′-hydroxyl groups). The conclusion that pyrimidine N(3) is involved in hydrogen bonding does not concur with our results that its neighboring C(2)=O forms a hydrogen bond acceptor feature. However, the frequently observed tautomeric forms of the pyrimidine base caused by a highly delocalized N(3) hydrogen atom may explain this minor discrepancy.

Both CoMFA and GOLPE models suggest that addition of a hydroxyl group at the 6-position of pyrimidine analogs would increase the inhibition of hCNT1; addition of a hydroxyl group at the 2-position of purine analogs would increase the inhibition of hCNT2; and addition of a hydroxyl group around the 3,5-position of pyrimidine (or 2,8-position of purine) analogs would increase the inhibition of hENT1.

A comparison of pharmacophoric features among the three models demonstrates that hENT1 is least sensitive to inhibitor modifications whereas hCNT2 is the most sensitive transporter, which is in agreement with experimental data. At first glance, it may seem extraordinary that hydrogen bond formation nearby 3′ carbon is a required feature for hENT1 affinity, even though a well characterized substrate such as 2′3′-dideoxyadenosine does not contain a carbonyl or hydroxyl group at this specific location. Upon further inspection of the DISCO features on 2′,3′-dideoxyadenosine (Fig. 4D), however, it becomes apparent that the hydrogen-bonding feature over 3′-C is actually derived from the lone pair at 5′-oxygen, whereas the hydrogen bond acceptor feature derives from the 3-amine of the base. Thus, based on experimental results alone, hydrogen bonding over 3′-C *seems* not to be an essential requirement for hENT1 inhibition, but our study shows that alternate features near this group may compensate for the lack of this moiety on the base. The fact that DISCO analysis discloses an alternate pathway for hydrogen bond formation near 3′-C demonstrates the ability of DISCO to discriminate alternative bioactive conformations of transport inhibitors. Thus, this analysis reveals the possibility of designing novel nucleoside analogs that retain affinity for hENT1 despite the absence of a requisite 3′-OH moiety.

TABLE 3
Experimental nucleoside transporter data and CoMFA predictions
Activities are shown as percentage inhibition.

		hCNT1(0.1 mM inhibitor, 1 μM[^{3}H]Thymidine)		hCNT2(0.1 mM inhibitor, 0.5 μM[^{3}H]Inosine)		hENT1(2.0 mM inhibitor, 10 μM[^{3}H]Uridine)	
n	Inhibitor	Activity	Prediction	Activity	Prediction	Activity	Prediction
1	1-Methyladenosine	59.5	63.7	82	66.3	36.5	34.9
2	2′,3′-Dideoxyadenosine	N/M	N/M	N/M	N/M	87.6	86.8
3	2′,3′-Dideoxycytidine	122.1	121.2	N/M	N/M	132	133.1
4	2′,3′-Dideoxyuridine	113.6	117.0	98.7	113.5	118.3	115.8
5	2-Chloro-2′-deoxyadenosine (Cladribine)	35.7	37.9	100.7	70.8	14.8	17.7
6	2-Chloroadenosine	50.8	52.9	88.9	76.2	16.4	15.2
7	2′-Deoxyadenosine	N/M	N/M	N/M	N/M	22.7	21.8
8	2′-Deoxyuridine	28.4	28.2	36.6	N/P	23.3	27.7
9	2-Fluoro-AF-adenine (Fludarabine)	74.5	N/P	104.2	90.6	N/M	N/M
10	3′-Deoxyadenosine	N/M	N/M	N/M	N/M	54.6	55.5
11	3-Deazauridine	63.9	69.7	101.9	N/P	97.4	95.7
12	3′-Deoxyuridine	110.7	108.9	105.8	108.3	60	60.0
13	3-Methyluridine	52.3	38.5	53.1	47.4	33.3	33.6
14	4-Thiouridine	17.8	25.0	19.6	28.0	31.8	30.1
15	5-Bromouridine	17.6	23.0	64	65.2	N/M	N/M
16	5-(2-Bromovinyl)-2′-deoxyuridine (Brivudin)	16.2	11.5	89.1	105.6	N/M	N/M
17	5′-Deoxyadenosine	73.5	N/P	95.9	93.9	29.8	31.7
18	5′-Deoxythymidine	54	57.0	N/M	N/M	32.9	29.4
19	5-Fluoro-2′-deoxyuridine (Floxuridine)	28.1	26.3	73.5	95.7	23.6	25.2
20	5-Fluoro-5′-deoxyuridine	65.4	58.7	110.1	99.1	N/M	N/M
21	5-Fluorouridine	28.5	37.2	31.2	23.0	29.1	28.0
22	5-Iodo-2′-deoxyuridine (Idoxuridine)	16	19.1	104.4	109.6	39.9	39.3
23	5-Iodouridine	16.1	7.4	101	N/P	20.4	20.7
24	5-(Trifluoromethyl)-2′-deoxyuridine (Trifluridin)	27.1	23.8	103.4	114.0	69.8	69.5
25	6-Azauridine	99.1	82.0	73.2	59.0	88.8	N/P
26	7-Deazaadenosine	42	41.5	61.6	56.9	15.1	16.6
27	8-Bromoadenosine	104.1	98.5	95.8	105.4	20.7	19.0
28	Adenosine	38.2	40.1	8.6	38.5	24.9	25.2
29	Acadesine	N/M	N/M	73	77.6	58.1	59.1
30	AF-adenine (Vidarabine)	89.3	91.4	99.7	85.8	32.7	34.6
31	AF-cytosine (Cytarabine)	131.4	134.7	N/M	N/M	49.7	48.5
32	Cytidine	33.6	28.7	N/M	N/M	38.2	35.5
33	2′,3′-Dideoxyinosine	N/M	N/M	95.7	87.6	126.6	125.7
34	Guanosine	N/M	N/M	18.2	26.7	35.9	35.4
35	Inosine	N/M	N/M	7.6	34.7	27.3	30.3
36	Lamivudine	143.3	143.8	N/M	N/M	106	103.5
37	N^6,N^6-Dimethyladenosine	74.3	N/P	97.2	85.8	13.5	13.9
38	N^6-Methyladenosine	47	52.1	86.9	81.8	N/M	N/M
39	Ribavirin	N/M	N/M	31	21.4	62.1	61.2
40	Stavudine	126.8	126.9	N/M	N/M	121.9	125.8
41	Thymidine	18.5	23.1	N/M	N/M	30	27.8
42	Uridine	26.2	32.4	18.3	23.2	29.8	30.5
43	UMP	N/M	N/M	N/M	N/M	123	124.1
44	Zidovudine	91.3	92.5	N/M	N/M	103	104.5

N/M, not experimentally measured; N/P, not predicted (outlier); AF, 9β-D-arabinofuranosyl.

TABLE 4
QSAR predictions of test compounds (CoMFA)

		Predicted	Actual
		% inhibition	
	hCNT1	0.1 mM inhibitor, 1 μM [^{3}H]thymidine	(1 mM inhibitor, 10 μM [^{3}H]uridine)
34	Guanosine	Inactive (114.0)	Inactive (~90)
45	Gemcitabine	Active (41.6)	Active (14)
46	2′-deoxycytidine	Active (53.1)	Active (~20)
	hCNT2	0.1 mM inhibitor, 0.5 μM [^{3}H]inosine	0.1 mM inhibitor, 10μM [^{3}H]uridine
46	2′-deoxycytidine	Inactive (95.1)	Inactive (96)
47	2′-deoxyguanosine	Active (44.7)	Active (3)
48	2′-deoxyinosine	Active (52.7)	Active (5)
49	5-methyluridine	Active (23.2)	Active (38)
50	AF-hypoxanthine	Inactive (106.7)	Active (20)
51	Hypoxanthine	Inactive (76.6)	Inactive (96)
	hENT1	2 mM inhibitor, 10 μM [^{3}H]uridine	IC_{50} mM, 1 μM [^{3}H]uridine
46	2′-deoxycytidine	Active (27.6)	Active (2.0)
48	5-methyluridine	Active (21.2)	Active (0.17)
20	5-fluoro-5′-deoxyuridine	Active (29.6)	Active (0.15)
52	5-bromo-2′-deoxyuridine	Active (41.7)	Active (0.24)
53	3′-deoxycytidine	Borderline Inactive/Active (56.3)	Borderline Inactive/Active (3.1)

AF, 9β-D-arabinofuranosyl.

A recent paper by Huang et al. (2002) describes the effective inhibition of nucleoside transport by the p38 MAPK inhibitors SB202474, SB203580, and SB203580-iodo (Fig. 8A). A structural analog of these compounds, SB220025, reportedly did not bear any effect on [^{3}H]uridine transport in K562 cells, which are known to express the equilibrative nucleoside transporter hENT1. These non-nucleoside analogs were subsequently built, energy-optimized, and aligned to uridine by overlapping the pentose ring to the imidazole moiety of all test structures. The alignment of the uridine ribose ring to the methylsulfoxide-phenyl (or methoxyphenyl) ring resulted from a field-fit energy minimization. Both imidazole and methylsulfoxide-phenyl moieties satisfy the hydrophobic features in hENT1 pharmacophore (Fig. 8B). Correspondingly, the imidazole 1-nitrogen in the MAPK inhibitors represents the hydrogen bond acceptor pharmacophore feature on the pentose ring of uridine. Based on pharmacophore features alone, the inactivity of SB220025 toward hENT1 can be explained by the substitution of the methylsulfoxide-phenyl group with a piperidine moiety on the imidazole nitrogen (Fig. 8A). In the active molecules, the fluoride (or iodo) atom and the highly electron deficient hydrogen atoms flanking the halide atom could act, respectively, as hydrogen bond acceptor and donor moieties, thus representing the corresponding pharmacophore groups over the 3-pentose position of uridine.

CoMFA predictions for hENT1 inhibition of SB203580, SB203580-Iodo, SB202474 and SB220025 were 57.7, 61.8, 64.4, and 68.6%, respectively. It is interesting to note that, even though the pharmacophore model effectively excluded SB220025, CoMFA-based predictions are unable to differentiate between the p38 MAPK inhibitors. Upon inspection of the CoMFA fields, however, it became apparent that the model is expectedly silent in areas where the training set lacks structural diversity (Fig. 8C). The piperidine ring of SB220025 protrudes into such a "silent" area of the model and, consequently, does not contribute negatively to its CoMFA-based prediction of hENT1 inhibition.

None of the MAPK inhibitors are predicted to be effective inhibitors of hCNT1 or hCNT2, based on both pharmacophore and CoMFA analyses (data not shown). Future studies are aimed at validating these predictions.

Conclusion

The structural features that are essential for nucleoside transporter affinity, transport, and inhibition have received increased attention from both a drug discovery and drug delivery standpoint. In the absence of a high-resolution protein structure, it is currently not feasible to directly design compounds that would either use or inhibit these transporter systems. In the study presented here, we examined the structural features of nucleoside transporter inhibitors and correlated these to their biological activity for each respective nucleoside transporter isoform. The resulting data present a roadmap toward recognizing the molecular characteristics that are required for inhibiting each individual transporter, their commonalities as well as the features that set them apart. For example, the models can distinguish effectively between inhibitors for different isoforms; e.g., 2-deoxycytidine was predicted to be an inhibitor for hENT1, but not hCNT2.

It should be pointed out that the current models are derived from inhibition data and thus that the models predominantly represent features important for nucleoside transporter *inhibition*. Although care should be taken in

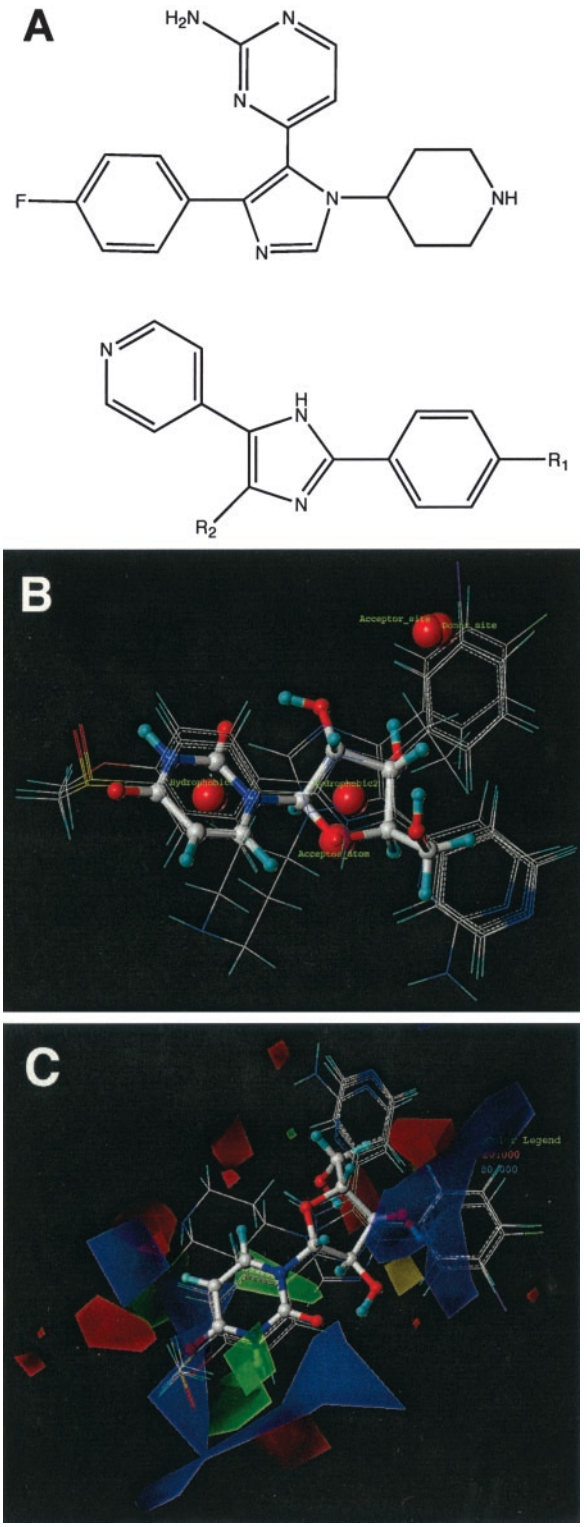

Fig. 8. A, structural formulas of p38 MAPK inhibitors; top, SB220025; SB202474, R_1 = OCH_3, R_2 = CH_2-CH_3; SB203580, R_1 = $SOCH_3$, R_2 = *p*-F-Ø; SB203580-iodo, R_1 = $SOCH_3$, R_2 = *m*-I-Ø. B, alignment of p38 MAPK inhibitors onto uridine together with the hENT1 pharmacophore points. C, relative position of the p38 MAPK inhibitor structures within the hENT1 CoMFA contours.

extrapolating these findings to predict nucleoside transporter *substrates*, invariably many of the active inhibitors in the current study have been shown to be substrates for the transporters as well. Therefore, it is not unreasonable to speculate that active inhibitors (i.e., >60% inhibition) may very well turn out to be good nucleoside transporter substrates, when validated in vitro.

The three-pronged approach of pharmacophore mapping and two independent multivariate 3D-QSAR methods represents an indirect examination of the nucleoside transporters' binding sites. From these models, we have been able to predict the inhibition of some compounds with the individual transporters, such as p38 MAPK inhibitors. Additional studies will indubitably improve the models and may ultimately diminish the intrinsic occurrence of false positives and negatives in each model (e.g., AF-hypoxanthine). This will require an iterative process of additional data input and evaluation of novel test compounds. In addition, the possibility of database mining in combination with de novo ligand design can be used to find lead compounds that may have affinity for nucleoside transporters or design novel chemical entities with these properties. In this respect, the use of a CoMFA-derived binding site cavity in combination with structure generating and docking algorithms, such as LeapFrog, will be an effective approach. Our future studies are aimed at further exploration of the binding site requisites of the respective nucleoside transporters to facilitate and optimize rational drug design.

Acknowledgments

We gratefully acknowledge Dr. Gabriele Cruciani (University of Perugia, Italy) for allowing us to use the GOLPE algorithm.

References

Bednarczyk D, Ekins S, Wikel JH, and Wright SH (2003) Influence of molecular structure on substrate binding to the human organic cation transporter, hOCT1. *Mol Pharmacol* **63:**489–498.

Bohacek RS and McMartin C (1992) Definition and display of steric, hydrophobic and hydrogen-bonding properties of ligand binding sites in proteins using Lee and Richards accessible surface: validation of a high-resolution graphical tool for drug design. *J Med Chem* **35:**1671–1684.

Cass CE, Young JD, and Baldwin SA (1998) Recent advances in the molecular biology of nucleoside transporters of mammalian cells. *Biochem Cell Biol* **76:**761–770.

Chandrasena G, Giltay R, Patil SD, Bakken A, and Unadkat JD (1997) Functional expression of human intestinal Na^+-dependent and Na^+- independent nucleoside transporters in *Xenopus laevis* oocytes. *Biochem Pharmacol* **53:**1909–1918.

Cramer SP, Patterson DE, and Bunce JD (1988) Comparative molecular field analysis (CoMFA). 1. Effect of shape on binding of steroids to carrier proteins. *J Am Chem Soc* **110:**5959–5967.

Ekins S, Kim RB, Leake BF, Dantzig AH, Schuetz EG, Lan LB, Yasuda K, Shepard RL, Winter MA, Schuetz JD, et al. (2002a) Application of three-dimensional quantitative structure-activity relationships of P-glycoprotein inhibitors and substrates. *Mol Pharmacol* **61:**974–981.

Ekins S, Kim RB, Leake BF, Dantzig AH, Schuetz EG, Lan LB, Yasuda K, Shepard RL, Winter MA, Schuetz JD, et al. (2002b) Three-dimensional quantitative structure-activity relationships of inhibitors of P-glycoprotein. *Mol Pharmacol* **61:**964–973.

Goodford PJ (1985) A computational procedure for determining energetically favorable binding sites on biologically important macromolecules. *J Med Chem* **28:**849–857.

Graham KA, Leithoff J, Coe IR, Mowles D, Mackey JR, Young JD, and Cass CE (2000) Differential transport of cytosine-containing nucleosides by recombinant human concentrative nucleoside transporter protein hCNT1. *Nucleosides Nucleotides Nucleic Acids* **19:**415–434.

Griffith DA and Jarvis SM (1996) Nucleoside and nucleobase transport systems of mammalian cells. *Biochim Biophys Acta* **1286:**153–181.

Horwitz JP, Massova I, Wiese TE, Besler BH, and Corbett TH (1994) Comparative molecular field analysis of the antitumor activity of 9H- thioxanthen-9-one derivatives against pancreatic ductal carcinoma 03. *J Med Chem* **37:**781–786.

Huang M, Wang Y, Collins M, Gu JJ, Mitchell BS, and Graves LM (2002) Inhibition of nucleoside transport by p38 MAPK inhibitors. *J Biol Chem* **277:**28364–28367.

Jarvis SM, Thorn JA, and Glue P (1998) Ribavirin uptake by human erythrocytes and the involvement of nitrobenzylthioinosine-sensitive (es)-nucleoside transporters. *Br J Pharmacol* **123:**1587–1592.

Kroemer RT and Hecht P (1995) Replacement of steric 6–12 potential-derived interaction energies by atom-based indicator variables in CoMFA leads to models of higher consistency. *J Comput Aided Mol Des* **9:**205–212.

Kroemer RT, Koutsilieri E, Hecht P, Liedl KR, Riederer P, and Kornhuber J (1998) Quantitative analysis of the structural requirements for blockade of the *N*-methyl-D-aspartate receptor at the phencyclidine binding site. *J Med Chem* **41:**393–400.

Lai Y, Bakken AH, and Unadkat JD (2002) Simultaneous expression of hCNT1-CFP and hENT1-YFP in Madin-Darby canine kidney cells. Localization and vectorial transport studies. *J Biol Chem* **277:**37711–37717.

Lang TT, Selner M, Young JD, and Cass CE (2001) Acquisition of human concentrative nucleoside transporter 2 (hcnt2) activity by gene transfer confers sensitivity to fluoropyrimidine nucleosides in drug-resistant leukemia cells. *Mol Pharmacol* **60:**1143–1152.

Loewen SK, Ng AM, Yao SY, Cass CE, Baldwin SA, and Young JD (1999) Identification of amino acid residues responsible for the pyrimidine and purine nucleoside specificities of human concentrative Na^+ nucleoside cotransporters hCNT1 and hCNT2. *J Biol Chem* **274:**24475–24484.

Lum PY, Ngo LY, Bakken AH, and Unadkat JD (2000) Human intestinal es nucleoside transporter: molecular characterization and nucleoside inhibitory profiles. *Cancer Chemother Pharmacol* **45:**273–278.

Mackey JR, Baldwin SA, Yound JD, and Cass CE (1998) Nucleoside transport and its significance for anticancer drug resistance. *Drug Resist Updat* **1:**310–324.

Martin YC, Bures MG, Danaher EA, DeLazzer J, Lico I, and Pavlik PA (1993) A fast new approach to pharmacophore mapping and its application to dopaminergic and benzodiazepine agonists. *J Comput Aided Mol Des* **7:**83–102.

Molina-Arcas M, Bellosillo B, Casado FJ, Montserrat E, Gil J, Colomer D, and Pastor-Anglada M (2003) Fludarabine uptake mechanisms in B-cell chronic lymphocytic leukemia. *Blood* **101:**2328–2334.

Ngo LY, Patil SD, and Unadkat JD (2001) Ontogenic and longitudinal activity of Na^+-nucleoside transporters in the human intestine. *Am J Physiol* **280:**G475–G481.

Pastor M, Cruciani G, and Clementi S (1997) Smart region definition: a new way to improve the predictive ability and interpretability of three-dimensional quantitative structure- activity relationships. *J Med Chem* **40:**1455–1464.

Patil SD, Ngo LY, and Unadkat JD (2000) Structure-inhibitory profiles of nucleosides for the human intestinal N1 and N2 Na^+-nucleoside transporters. *Cancer Chemother Pharmacol* **46:**394–402.

Patil SD and Unadkat JD (1997) Sodium-dependent nucleoside transport in the human intestinal brush- border membrane. *Am J Physiol* **272:**G1314–G1320.

Schaal W, Karlsson A, Ahlsen G, Lindberg J, Andersson HO, Danielson UH, Classon B, Unge T, Samuelsson B, Hulten J, et al. (2001) Synthesis and comparative molecular field analysis (CoMFA) of symmetric and nonsymmetric cyclic sulfamide HIV-1 protease inhibitors. *J Med Chem* **44:**155–169.

Swaan PW, Koops BC, Moret EE, and Tukker JJ (1998) Mapping the binding site of the small intestinal peptide carrier (PepT1) using comparative molecular field analysis. *Recept Channels* **6:**189–200.

Swaan PW, Szoka FC Jr, and Oie S (1997) Molecular modeling of the intestinal bile acid carrier: a comparative molecular field analysis study. *J Comput Aided Mol Des* **11:**581–588.

Vickers MF, Kumar R, Visser F, Zhang J, Charania J, Raborn RT, Baldwin SA, Young JD, and Cass CE (2002) Comparison of the interaction of uridine, cytidine and other pyrimidine nucleoside analogues with recombinant human equilibrative nucleoside transporter 2 (hENT2) produced in Saccharomyces cerevisiae. *Biochem Cell Biol* **80:**639–644.

Viswanadhan VN, Ghose AK, and Weinstein JN (1990) Mapping the binding site of the nucleoside transporter protein: a 3D-QSAR study. *Biochim Biophys Acta* **1039:**356–366.

Zhang EY, Knipp GT, Ekins S, and Swaan PW (2002) Structural biology and function of solute transporters: implications for identifying and designing substrates. *Drug Metab Rev* **34:**709–750.

Zhang J, Visser F, Vickers MF, Lang T, Robins MJ, Nielsen LPC, Nowak I, Baldwin SA, Young JD, and Cass CE (2003) Uridine binding motifs of human concentrative nucleoside transporters 1 and 3 produced in *Saccharomyces cerevisiae. Mol Pharmacol* **64:**1512–1520.

Address correspondence to: Peter W. Swaan, Department of Pharmaceutical Sciences, University of Maryland, 20 Penn Street, Baltimore, MD 21202. E-mail: pswaan@rx.umaryland.edu